Science Bulletin 71 (2026) 745–751

Contents lists available at ScienceDirect

Science Bulletin

journal homepage: www.elsevier.com/locate/scib

Article

Controllable deterministic quantum teleportation of multiple sideband qumodes

Na Wang [a,1], Meihong Wang [a,b,1], Chun Ma [a], Xuefan Xing [a], Dongmei Han [a,b], Xiaolong Su [a,b,*]

[a] State Key Laboratory of Quantum Optics Technologies and Devices, Institute of Opto-Electronics, Shanxi University, Taiyuan 030006, China
[b] Collaborative Innovation Center of Extreme Optics, Shanxi University, Taiyuan 030006, China

ARTICLE INFO

Article history:
Received 3 September 2025
Received in revised form 20 November 2025
Accepted 23 December 2025
Available online 30 December 2025

Keywords:
Quantum communication
Quantum teleportation
Quantum entanglement
Sideband qumode

ABSTRACT

As an important quantum communication protocol, quantum teleportation has broad applications in quantum information science and technology. For the application, it is essential to enhance the ability of quantum teleportation by teleporting multiple quantum states simultaneously. Here, we experimentally demonstrate deterministic quantum teleportation of multiple sideband qumodes of coherent states, which corresponds to teleporting multiple quantum states simultaneously, with the assistance of continuous-variable (CV) quantum entanglement. By fine-tuning the phases of two classical channels according to different adjustable frequencies, we successfully realize deterministic CV quantum teleportation with up to 5 sideband qumodes simultaneously within the frequency bandwidth of 24 MHz. We show that the number of teleported multiple qumodes is controllable by changing the phases of two classical channels. The obtained fidelities of output multiple qumodes are around 70%, which are all beyond the non-cloning limit. The results present a novel method for quantum teleportation of multiple quantum states simultaneously and take a crucial step in enhancing the teleporting ability of quantum teleportation.

© 2025 Science China Press. Published by Elsevier B.V. and Science China Press. All rights are reserved, including those for text and data mining, AI training, and similar technologies.

1. Introduction

As a typical entanglement-based quantum communication protocol, quantum teleportation realizes the transfer of an unknown quantum state between distant users with the assistance of shared entanglement and classical communication [1,2]. Since the first experimental demonstration of it [3], quantum teleportation has been realized via different quantum systems, including photonic qubits [4–9], nuclear magnetic resonance [10], optical modes [11,12], atomic ensembles [13–15], trapped atoms [16–18], solid-state quantum system [19–22], and superconducting chips [23]. Besides the point-to-point quantum communication, quantum teleportation has also been extended to quantum network communication [24–28] and has essential application in the distributed quantum computing [29–32].

Typically, only one unknown quantum state is teleported at a time in quantum teleportation. If multiple degree-of-freedom of a quantum state or multiple quantum states can be teleported simultaneously by implementing quantum teleportation once, the teleporting ability of it will be enhanced significantly. Much effort has been dedicated to enhancing the teleporting ability of quantum teleportation in recent years, for example, quantum teleportation of photons carrying orbital angular momentum [33,34] and high-dimensional state [35,36] have been experimentally demonstrated. The multiplexed optical frequency comb [37] and orbital angular momentum multiplexed channels [38,39] have also been applied in quantum teleportation. Recently, all-optical quantum teleportation of four degrees of freedom has been experimentally demonstrated, where azimuthal and radial indexes of Laguerre-Gaussian mode, frequency, and polarization are applied [40].

Continuous-variable (CV) quantum teleportation has the advantage of determinacy since the generation of entanglement, realization of joint measurement, and homodyne detection are all deterministic. Various quantum states, including coherent [41,42], squeezed [43,44], and non-Gaussian states [45,46], have been experimentally teleported in CV quantum teleportation. Up to now, most CV quantum teleportation is limited to teleporting a sideband qumode of the optical field at a time. When teleporting N quantum states simultaneously in a quantum communication task, N traditional CV quantum teleportation systems based on N

* Corresponding author.
E-mail address: suxl@sxu.edu.cn (X. Su).
[1] These authors contributed equally to this work.

https://doi.org/10.1016/j.scib.2025.12.047
2095-9273/© 2025 Science China Press. Published by Elsevier B.V. and Science China Press. All rights are reserved, including those for text and data mining, AI training, and similar technologies.

entangled states are required, which increases the consumption of quantum resources and total cost of quantum communication systems. Thus, it is essential to develop a new technology to save the quantum resource and reduce the cost. If multiple sideband qumodes (N quantum states at different sideband frequencies) can be teleported with one CV quantum teleportation system at once, which will significantly enhance the ability of CV quantum teleportation and reduce the cost. However, it remains a challenge for teleporting multiple sideband qumodes simultaneously.

Here, we experimentally demonstrate controllable deterministic quantum teleportation of multiple sideband qumodes simultaneously. By controlling the relative phase in the classical channel and Alice's measurement system in CV quantum teleportation, we show that multiple sideband qumodes with odd or even times of the basic sideband frequency, which is the sideband frequency used to calibrate the classical channel, are teleported simultaneously. Furthermore, we experimentally demonstrate quantum teleportation of up to 5 sideband qumodes simultaneously within the frequency bandwidth of 24 MHz and show that the number of teleportable sideband qumodes is limited by the bandwidth of the CV quantum teleportation system. Our results reveal the phenomenon that multiple sideband quantum states can be teleported simultaneously, and the number of teleportable sideband qumodes in CV quantum teleportation is controllable by tuning the phase of the classical channel.

2. The principle

In CV quantum information processing, the information is encoded in the amplitude and phase quadratures of photonics harmonic oscillators [47], which are expressed by $\hat{X}=\hat{a}+\hat{a}^{\dagger}$ and $\hat{P}=(\hat{a}-\hat{a}^{\dagger})/i$, respectively. In this case, variances of amplitude and phase quadratures for a vacuum state are $V_{\hat{X}_0}=V_{\hat{P}_0}=V_0=1$, where the subscript 0 represents a vacuum state. The quantum correlation and anti-correlation of the frequency-dependent CV Einstein-Podolsky-Rosen (EPR) entangled state are

$$\Delta^2\left[\hat{X}_{\mathrm{A}}(v)+\hat{X}_{\mathrm{B}}(v)\right]=\Delta^2\left[\hat{P}_{\mathrm{A}}(v)-\hat{P}_{\mathrm{B}}(v)\right]=2e^{-2r}, \tag{1}$$

where v is the sideband frequency, r is the squeezing parameter. As shown in Fig. 1, the entangled modes $\hat{A}$ and $\hat{B}$ of a CV EPR entangled state are sent to Alice and Bob, respectively, to implement quantum teleportation of multiple sideband qumodes.

Alice couples the input mode $\hat{I}(v)=\hat{X}_{\mathrm{in}}(v)+\mathrm{i}\hat{P}_{\mathrm{in}}(v)$ and mode $\hat{A}(v)$ on a 1:1 beamsplitter and measures the output modes $\hat{C}(v)=\left[\hat{I}(v)+\hat{A}(v)\right]/\sqrt{2}$ and $\hat{D}(v)=\left[\hat{I}(v)-\hat{A}(v)\right]/\sqrt{2}$ with two homodyne detectors (HD1 and HD2), respectively. The corresponding measurement results $x_{\theta_1}(v)=\hat{X}_{\mathrm{C}}(v)\cos\theta_1+\hat{P}_{\mathrm{C}}(v)\sin\theta_1$, $x_{\theta_2}(v)=\hat{X}_{\mathrm{D}}(v)\cos\theta_2+\hat{P}_{\mathrm{D}}(v)\sin\theta_2$, where θ_1 and θ_2 are phase differences in HD1 and HD2 respectively, are fed forward to Bob through classical channels with gain g and phase ϕ. Bob implements the phase space displacement operation by modulating the mode $\hat{B}(v)$ with electro-optical amplitude and phase modulators (EOMx and EOMp). Victor measures the output mode $\hat{B}'(v)$, which is given by

$$\hat{B}'(v)=\hat{B}(v)+\mathrm{e}^{\mathrm{i}\phi}\left[\sqrt{2}gx_{\theta_1}(v)+\mathrm{i}\sqrt{2}gx_{\theta_2}(v)\right], \tag{2}$$

where ϕ is the phase in the classical channel. The amplitude and phase quadratures of the output state are

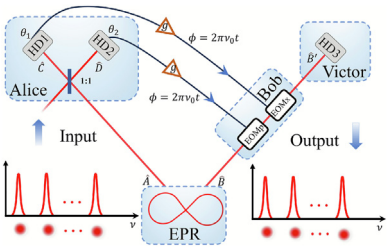

Fig. 1. The principle of controllable deterministic quantum teleportation of multiple sideband qumodes. By controlling the phases in classical channels for the basic sideband qumode v_0 and the phase differences of Alice's homodyne detection systems, multiple sideband qumodes are teleported. g, gain in the classical channel; EOMx and EOMp, electro-optical amplitude and phase modulators; HD, homodyne detector.

$$\begin{aligned}\hat{X}_{\mathrm{B}'}(v)&=\hat{X}_{\mathrm{B}}(v)+\sqrt{2}g\cos\phi x_{\theta_1}(v)-\sqrt{2}g\sin\phi x_{\theta_2}(v),\\ \hat{P}_{\mathrm{B}'}(v)&=\hat{P}_{\mathrm{B}}(v)+\sqrt{2}g\cos\phi x_{\theta_2}(v)+\sqrt{2}g\sin\phi x_{\theta_1}(v),\end{aligned} \tag{3}$$

respectively. Since the phase in the classical channel depends on frequency, we choose the phase $\phi_0=2\pi v_0 t=(2n+1)\pi$ (n is an integer) and gain $g=1$ for a basic sideband frequency v_0. In this case, the total gain $g\cos\phi_0=-1$ and the last term in Eq. (3) is canceled since $g\sin\phi_0=0$. For an arbitrary qumode with sideband frequency v, the phase in the classical channel is given by

$$\phi=2\pi vt=2\pi v\frac{(2n+1)\pi}{2\pi v_0}=\frac{v}{v_0}(2n+1)\pi. \tag{4}$$

Case I. If the sideband frequencies of arbitrary qumodes are even times of the basic sideband frequency $v=2nv_0$, we have $\cos\phi=1$. When we set $\theta_1=0,\theta_2=\pi/2$, the amplitude and phase quadratures of the output state turn into

$$\begin{aligned}\hat{X}_{\mathrm{B}'}(v)&=\hat{X}_{\mathrm{B}}(v)+\hat{X}_{\mathrm{A}}(v)+\hat{X}_{\mathrm{in}}(v),\\ \hat{P}_{\mathrm{B}'}(v)&=\hat{P}_{\mathrm{B}}(v)-\hat{P}_{\mathrm{A}}(v)+\hat{P}_{\mathrm{in}}(v).\end{aligned} \tag{5}$$

According to the quantum correlation of CV EPR entangled state in Eq. (1), when the squeezing parameter $r\to\infty$, the multiple input states with even times of the basic sideband frequency $v=2nv_0$ are successfully teleported.

Case II. If sideband frequencies of arbitrary qumodes are odd times of the basic sideband frequency $v=(2n+1)v_0$, we have $\cos\phi=-1$. When we set $\theta_1=\pi,\theta_2=-\pi/2$, the amplitude and phase quadratures of the output state also turn into Eq. (5), which means that multiple input states with odd times of the basic sideband frequency $v=(2n+1)v_0$ are successfully teleported.

From the above analysis, it can be seen that the teleportable sideband qumodes with odd or even times of the basic sideband frequency can be controlled by choosing the phase differences θ_1 and θ_2 when the basic sideband frequency is fixed. Since the generated CV EPR entangled state has a bandwidth limitation of BW, the teleportable number of sideband qumodes is limited to $N=1+\lfloor\frac{BW-v_1}{\Delta v}\rfloor$, where v_1 represents the frequency of the first teleported qumode, Δv is the frequency interval between the teleported qumodes, and $\lfloor.\rfloor$ denotes the round down symbol. For Case I and Case II, the teleportable numbers of sideband qumodes are $N_1=1+\lfloor\frac{BW}{2v_0}-1\rfloor$ and $N_2=1+\lfloor\frac{BW}{2v_0}-\frac{1}{2}\rfloor$, respectively, where the frequency intervals in the two cases are both $\Delta v=2v_0$. Therefore, by changing the basic sideband frequency v_0 and precisely controlling the phase of a selected basic sideband frequency to satisfy the requirement of $(2n+1)\pi$ in classical channels, we can control the number of multiple sideband qumodes teleported in CV quantum teleportation.

3. Experimental setup

As shown in Fig. 2, the CV EPR entangled state is generated from a non-degenerate optical parametric amplifier (NOPA) [48–51]. When it is operated at the parametric deamplification status, where the relative phase between the pump and seed beams of NOPA is locked to π, the EPR state with anti-correlated amplitude quadrature and correlated phase quadrature, as shown in Eq. (1), is prepared. The measured squeezing level varies in 3–5 dB in the frequency range of 2.5–24 MHz (Fig. S1 online). To realize the displacement of mode $\widehat{B}$, the measurement results of HD1 and HD2 are fed forward to two coherent beams through classical channels with EOMx and EOMp, respectively. Bob couples mode $\widehat{B}$ and the phase modulated coherent beam on a 99:1 beamsplitter and then couples the amplitude modulated coherent beam on another 99:1 beamsplitter. The phase differences on 99:1 beamsplitters are locked to 0. The output state is verified by HD3 at Victor's station.

In this experiment, the most crucial part is the adjustment of gain and phase in classical channels, which are implemented by adjusting the power amplifiers, cable (delay), and attenuators. To do this, the EPR entangled state is replaced by the coherent light. Firstly, the gain $g = 1$ in the classical channel is realized by adjusting the variable attenuator in classical channels to make sure the observed noise power of the output state is 4.77 dB above the shot noise level (SNL), which corresponds to the classical limit since two units of vacuum noise are added into the output state when the input state is vacuum state in CV quantum teleportation [41]. Secondly, we adjust the phase in classical channels by modulating a classical signal at the basic sideband frequency ν_0 and adjusting the cable length to control the phase. When the cancellation of classical signals is observed by HD3, it means that the phase $\phi_0 = 2\pi\nu_0 t = (2n+1)\pi$ for a basic sideband frequency ν_0 is realized (see Fig. S2 (online)).

4. Results

After adjusting the classical channel for basic sideband frequency $\nu_0 = 2.5$ MHz, we perform quantum teleportation with an EPR entangled state when the pump light is injected into the NOPA. When the phase differences of HD1 and HD2 are locked to $\theta_1 = 0, \theta_2 = \pi/2$ in Case I, the measured noise power spectrum of amplitude and phase quadratures of output state are shown in Fig. 3a and b, respectively. It is obvious that 4 sideband qumodes at frequencies 5, 10, 15, and 20 MHz are teleported successfully, which are all even times of the basic sideband frequency 2.5 MHz. When the phase differences of HD1 and HD2 are locked to $\theta_1 = \pi, \theta_2 = -\pi/2$ in Case II, the measured noise power spectrum of amplitude and phase quadratures of output state are shown in Fig. 3c and d. It is obvious that 5 sideband qumodes at frequencies 2.5, 7.5, 12.5, 17.5, and 22.5 MHz are teleported successfully, which are odd times of the basic sideband frequency 2.5 MHz.

The controllability of the number of the teleportable sideband qumodes is obtained by changing the basic sideband frequency ν_0. Here, we take Case II as an example to demonstrate the controllability of the number of the teleportable sideband qumodes. When the basic sideband frequency $\nu_0 = 3.5$ MHz, the measured noise power spectra of amplitude and phase quadratures of output state are shown in Fig. 4a and b, where 3 sideband qumodes at frequencies 3.5, 10.5, and 17.5 MHz are teleported successfully. When the basic sideband frequency $\nu_0 = 3$ MHz, the measured noise power spectra of amplitude and phase quadratures of output state are shown in Fig. 4c and d, where 4 sideband qumodes at frequencies 3, 9, 15, and 21 MHz are teleported successfully.

To obtain the full information of multiple sideband qumodes simultaneously, we reconstruct the Wigner functions of 5 output sideband qumodes simultaneously when the basic sideband frequency $\nu_0 = 2.5$ MHz is chosen. The alternating current signal from

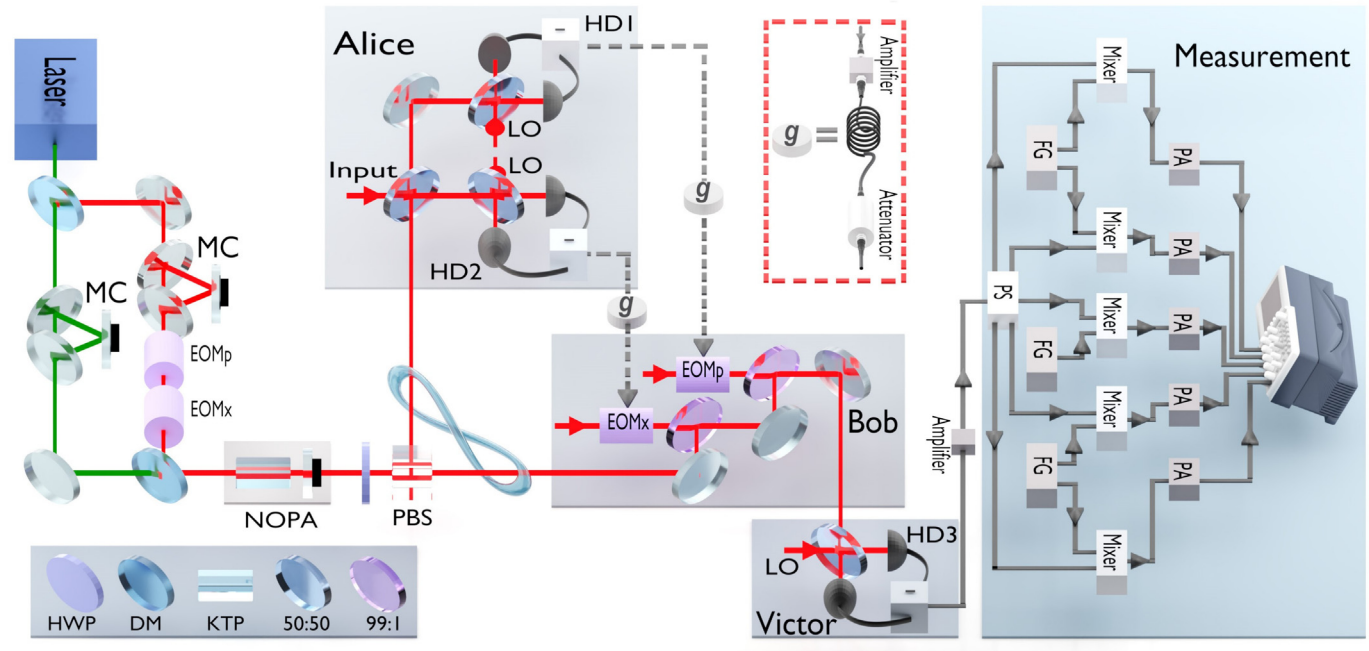

Fig. 2. Experimental setup. Alice's measurement results are fed forward to Bob through classical channels which consist of power amplifiers, cable (delay), and attenuators. The gain and phase in classical channels are calibrated for the basic sideband frequency by adjusting the classical signal added on the electro-optical amplitude and phase modulators (EOMx and EOMp) in front of non-degenerate optical parametric amplifier (NOPA) and components in classical channels. The alternating current signal of HD3 is split into five channels by power splitters (PS), then passes through the mixer and preamplifier (PA) to reconstruct the Wigner functions of 5 sideband qumodes. MC, mode cleaner; DM, dichroic mirror; PBS, polarization beam splitter; HWP, half wave plate; KTP, potassium titanyl phosphate; LO, local oscillator; FG, function generator.

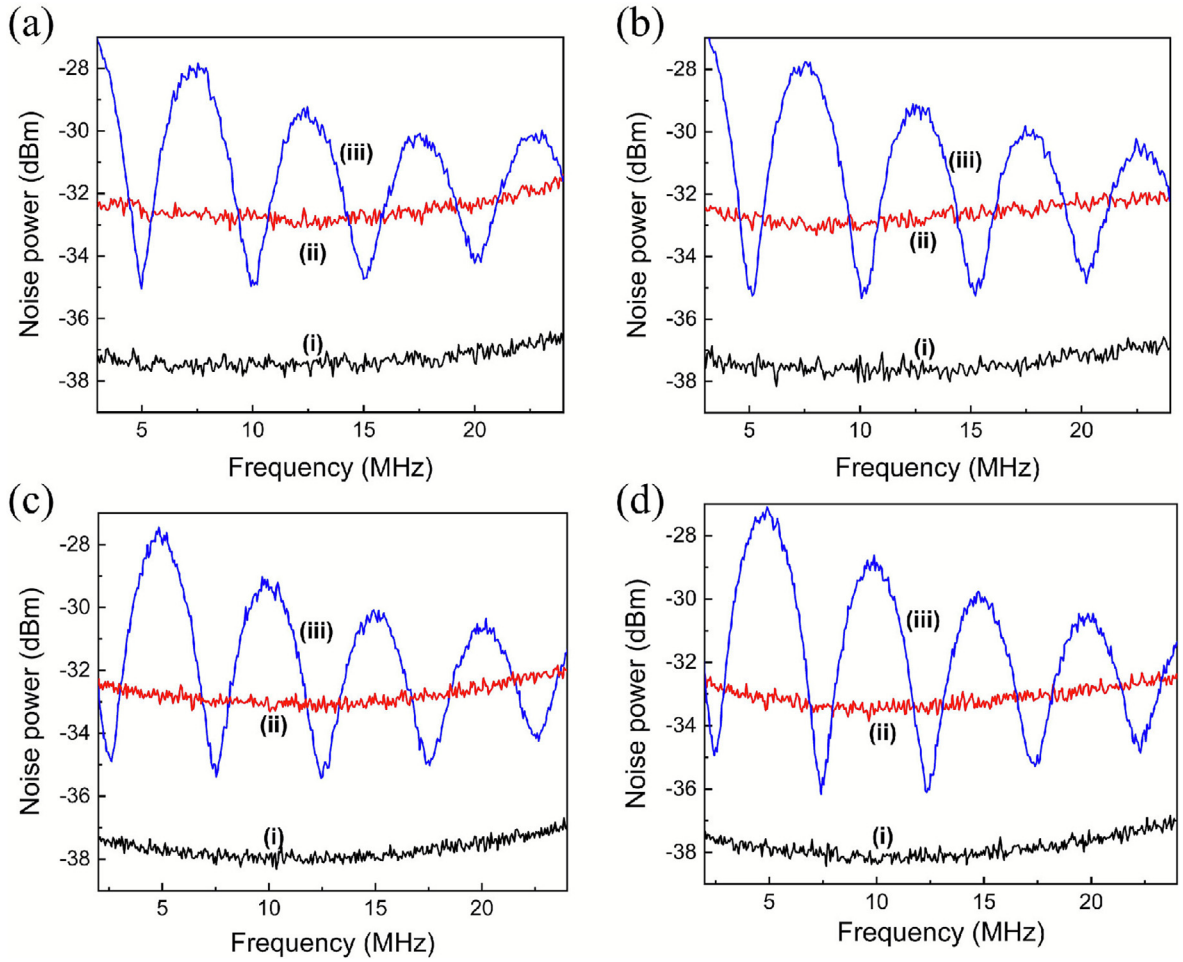

Fig. 3. The measured noise power spectrum of output sideband qumodes when the basic sideband frequency $\nu_0 = 2.5$ MHz is chosen. (a, b) Noise power spectra of amplitude and phase quadratures in Case I; (c, d) noise power spectra of amplitude and phase quadratures in Case II. Traces (i), (ii) and (iii) are shot noise level, classical limit, and output state, respectively. Resolution bandwidth of 100 kHz and video bandwidth of 300 Hz are chosen for the spectrum analyzer.

HD3 is split into five channels by power splitters and then mixed with local reference signals of 2.5, 7.5, 12.5, 17.5, and 22.5 MHz, and then filtered by low-pass filters with a bandwidth of 30 kHz and amplified 10 times (low-noise preamplifier, SRS, SR560) to demodulate the output 5 frequency sidebands, as shown in Fig. 2. The time domain data of quadratures are recorded simultaneously by a digital storage oscilloscope at the sampling rate of 500 kS/s. The reconstructed Wigner function of the input state is presented in Fig. 5a, while those for the output states at 2.5, 7.5, 12.5, 17.5, and 22.5 MHz are shown in Fig. 5b–f. The detailed purity, the mean values of the amplitude and phase quadratures for each sideband-frequency input and output states can be found in Supplementary materials S4.

The performance of quantum teleportation of a coherent state is quantified by the fidelity, which quantifies the overlap between the input and output states

$$F = \frac{2}{\sqrt{(1+\sigma_W^x)(1+\sigma_W^p)}}, \tag{6}$$

where σ_W^x and σ_W^p are the variances of amplitude and phase quadratures, respectively. After obtaining the σ_W^x and σ_W^p from the measured noise power in Figs. 3 and 4, the experimental fidelities of multiple sideband qumodes are calculated based on Eq. (6), which are all beyond the classical limit (0.5) and non-cloning limit (0.67) [52,53], as shown in Table 1. The fidelities obtained from the measured noise power and the reconstructed Wigner functions both confirm the successful quantum teleportation of multiple sideband qumodes.

5. Discussion and conclusion

In summary, we propose and demonstrate controllable deterministic CV quantum teleportation of multiple sideband qumodes simultaneously. Compared with previous CV quantum teleportation of a single sideband qumode, we realize the quantum teleportation of multiple sideband qumodes by employing the intrinsic phase-periodicity and the frequency dependence of phase, i.e., the phase in the classical channel changes with frequency under the same delay. While broadband quantum teleportation within a 12 MHz bandwidth has been implemented in Refs. [43,44] for non-Gaussian states by introducing appropriate optical delay lines, our frequency- and number-controllable quantum teleportation scheme enables selecting the targeted quantum sideband qumodes at user-defined frequencies.

It is interesting and worthwhile to explore the potential applications of the developed quantum teleportation technique in a multi-user, frequency-division multiplexing quantum communication network. In a quantum network, a quantum server (Alice) can realize CV quantum teleportation of quantum states at multiple sideband

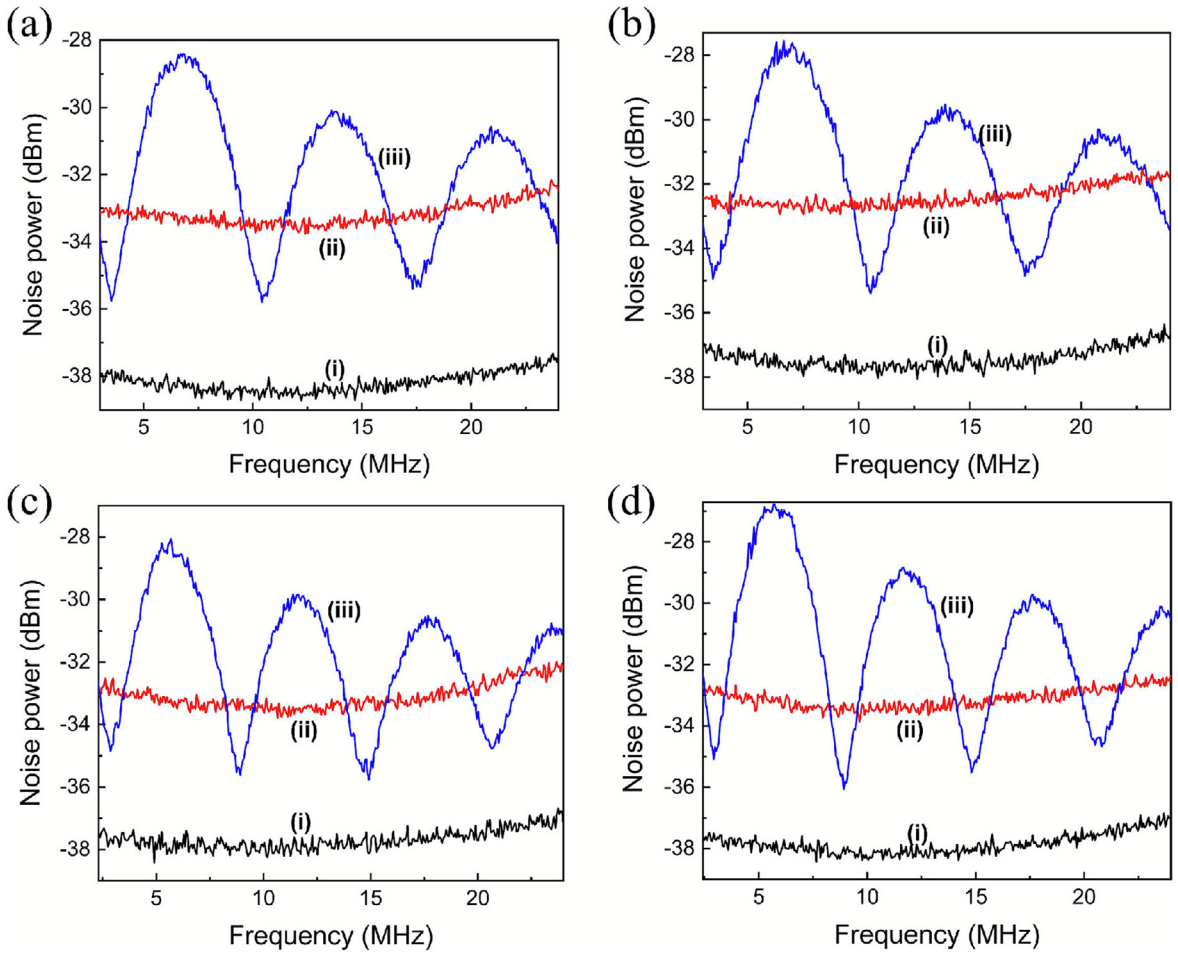

Fig. 4. The measured noise power spectra of different numbers of sideband qumodes. (a, b) Noise power spectra of amplitude and phase quadratures with $v_0 = 3.5$ MHz; (c, d) noise power spectra of amplitude and phase quadratures with $v_0 = 3$ MHz. Traces (i), (ii) and (iii) are shot noise level, classical limit, and output state, respectively. Resolution bandwidth of 100 kHz and video bandwidth of 300 Hz are chosen for the spectrum analyzer.

frequencies simultaneously to multiple users. By combining classical communication and quantum teleportation, the teleportation of multiple quantum states carrying classical information can be implemented in the quantum network. For example, a multi-channel quantum key distribution within a frequency-division multiplexing scheme and the teleportation of multiple images encoded at different sideband frequencies may be implemented.

We demonstrate that multiple qumodes with even or odd times of basic sideband frequency are teleported by controlling the phases of homodyne detection at Alice's station. Up to 5 sideband qumodes are teleported within 24 MHz frequency range by changing the basic sideband frequency and the phase in the classical channels. The number of teleported sideband qumodes is related to the basic sideband frequency and the bandwidth of the CV quantum teleportation system, including the bandwidth of the entanglement resource, the bandwidth of the classical channels, and the bandwidth of the homodyne detectors. The number of teleported sideband qumodes can be further increased by increasing the bandwidth of NOPA and measurement system, which is helpful to improve the scalability of quantum teleportation. Furthermore, the fidelity of quantum teleportation can be improved by increasing the squeezing level of the squeezed state. Our results provide a new method to teleport multiple sideband qumodes in CV quantum teleportation, which enhances the teleporting ability of quantum teleportation and takes a crucial step toward efficient CV entanglement-based quantum communication.

Conflict of interest

The authors declare that they have no conflict of interest.

Acknowledgments

This work was supported by the Quantum Science and Technology-National Science and Technology Major Project (2024ZD0302403), the National Natural Science Foundation of China (12434015 and 62275145), the Fundamental Research Program of Shanxi Province (202403021224001), and the Fund for Shanxi "331 Project" Key Subjects Construction.

Author contributions

Xiaolong Su conceived the original idea. Na Wang and Meihong Wang performed theoretical analysis and calculations. Na Wang, Chun Ma, Xuefan Xing, and Dongmei Han performed the experiment. Na Wang and Meihong Wang analyzed the experimental data. Na Wang, Meihong Wang, and Xiaolong Su wrote the paper.

Appendix A. Supplementary material

Supplementary data to this article can be found online at https://doi.org/10.1016/j.scib.2025.12.047.

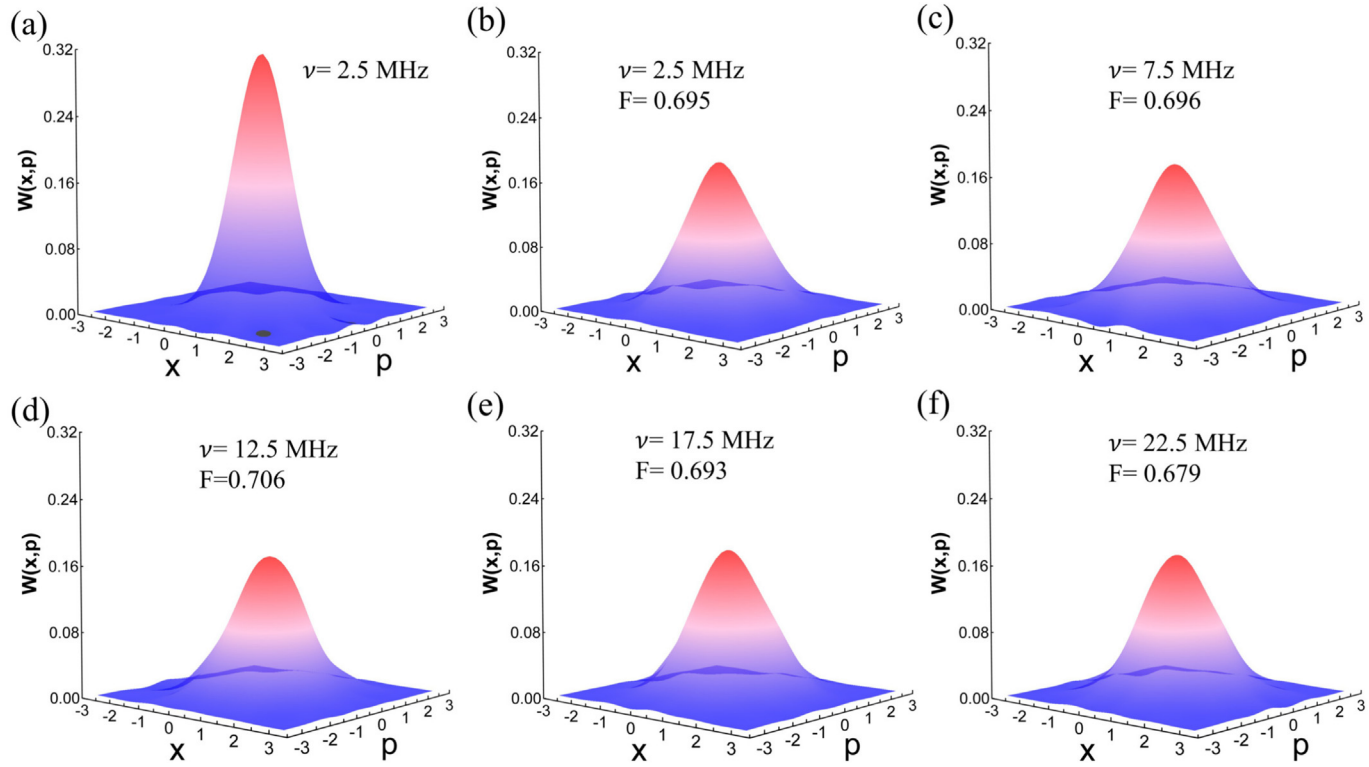

Fig. 5. Wigner functions of input state and output state at different frequencies of sideband. (a) Reconstructed Wigner functions of input state. (b–f) Reconstructed Wigner functions of output state with frequencies 2.5, 7.5, 12.5, 17.5, and 22.5 MHz sidebands, respectively. A sample size of 20000 data points is used for quantum state tomography.

Table 1
Experimental fidelities of multiple sideband qumodes with different basic sideband frequencies.

Basic sideband frequency (MHz)	Sideband frequency (MHz)	Fidelity	Basic sideband frequency (MHz)	Sideband frequency (MHz)	Fidelity
	5	0.717 ± 0.017		2.5	0.702 ± 0.010
	10	0.738 ± 0.007		7.5	0.742 ± 0.005
2.5	15	0.733 ± 0.017	2.5	12.5	0.745 ± 0.010
	20	0.728 ± 0.001		17.5	0.721 ± 0.006
				22.5	0.683 ± 0.010
	3	0.708 ± 0.006		3.5	0.720 ± 0.020
3	9	0.712 ± 0.012	3.5	10.5	0.742 ± 0.005
	15	0.732 ± 0.013		17.5	0.703 ± 0.012
	21	0.70 ± 0.010			

References

[1] Pirandola S, Eisert J, Weedbrook C, et al. Advances in quantum teleportation. Nat Photon 2015;9:641.
[2] Hu X-M, Guo Y, Liu B-H, et al. Progress in quantum teleportation. Nat Rev Phys 2023;5:339.
[3] Bouwmeester D, Pan J-W, Mattle K, et al. Experimental quantum teleportation. Nature 1997;390:575.
[4] Lombardi E, Sciarrino F, De Martini F, et al. Teleportation of a vacuum–one-photon qubit. Phys Rev Lett 2002;88:070402.
[5] Marcikic I, de Riedmatten H, Tittel W, et al. Long distance quantum teleportation of qubits from photons at 1300 nm to photons at 1550 nm wavelength. Nature 2003;421:509.
[6] Yin J, Ren J-G, Lu H, et al. Quantum teleportation and entanglement distribution over 100-kilometre free-space channels. Nature 2012;488:185.
[7] Ma X-S, Herbst T, Scheidl T, et al. Quantum teleportation over 143 kilometres using active feed-forward. Nature 2012;489:269.
[8] Ren J-G, Xu P, Yong H-L, et al. Ground-to-satellite quantum teleportation. Nature 2017;549:70.
[9] Chen Y-A, Zhang Q, Chen T-Y, et al. An integrated space-to-ground quantum communication network over 4,600 kilometres. Nature 2021;589:214.
[10] Nielsen MA, Knill E, Laflamme R, et al. Complete quantum teleportation using nuclear magnetic resonance. Nature 1998;396:52.
[11] Furusawa A, Sørensen JL, Braunstein SL, et al. Unconditional quantum teleportation. Science 1998;282:706.
[12] Huo M, Qin J, Cheng J, et al. Deterministic quantum teleportation through fiber channels. Sci Adv 2018;4:eaa9401.
[13] Sherson JF, Krauter H, Olsson RK, et al. Quantum teleportation between light and matter. Nature 2006;443:557.
[14] Chen Y-A, Chen S, Yuan Z-S, et al. Memory-built-in quantum teleportation with photonic and atomic qubits. Nat Phys 2008;4:103.
[15] Nölleke C, Neuzner A, Reiserer A, et al. Efficient teleportation between remote single-atom quantum memories. Phys Rev Lett 2013;110:140403.
[16] Barrett MD, Chiaverini J, Schaetz T, et al. Deterministic quantum teleportation of atomic qubits. Nature 2004;429:737.
[17] Riebe M, Häffner H, Roos CF, et al. Deterministic quantum teleportation with atoms. Nature 2004;429:734.
[18] Olmschenk S, Matsukevich DN, Maunz P, et al. Quantum teleportation between distant matter qubits. Science 2009;323:486.
[19] Gao W-B, Fallahi P, Togan E, et al. Quantum teleportation from a propagating photon to a solid-state spin qubit. Nat Commun 2013;4:2744.
[20] Bussières F, Clausen C, Tiranov A, et al. Quantum teleportation from a telecom-wavelength photon to a solid-state quantum memory. Nat Photon 2014;8:775.
[21] Steffen L, Salathe Y, Oppliger M, et al. Deterministic quantum teleportation with feed-forward in a solid state system. Nature 2013;500:319.
[22] Pfaff W, Hensen BJ, Bernien H, et al. Unconditional quantum teleportation between distant solid-state quantum bits. Science 2014;345:532.
[23] Qiu J, Liu Y, Hu L, et al. Deterministic quantum state and gate teleportation between distant superconducting chips. Sci Bull 2025;70:351–8.
[24] Su X, Tian C, Deng X, et al. Quantum entanglement swapping between two multipartite entangled states. Phys Rev Lett 2016;117:240503.

[25] Sun Q-C, Mao Y-L, Chen S-J, et al. Quantum teleportation with independent sources entanglement distribution over a network. Nat Photon 2016;10:671.
[26] Valivarthi R, Puigibert MLG, Zhou Q, et al. Quantum teleportation across a metropolitan fibre network. Nat Photon 2016;10:676.
[27] Ren S, Han D, Wang M, et al. Continuous variable quantum teleportation and remote state preparation between two space-separated local networks. Sci China Inf Sci 2024;67:142502.
[28] Wang N, Wang M, Tian C, et al. Experimental demonstration of quantum steering swapping with Gaussian entangled states. Laser Photon Rev 2024;18:2300653.
[29] Wehner S, Elkouss D, Hanson R, et al. Quantum internet: a vision for the road ahead. Science 2018;362:6412.
[30] Chou KS, Blumoff JZ, Wang CS, et al. Deterministic teleportation of a quantum gate between two logical qubits. Nature 2018;561:368.
[31] Wan Y, Kienzler D, Erickson SD, et al. Quantum gate teleportation between separated qubits in a trapped-ion processor. Science 2019;364:875.
[32] Daiss S, Langenfeld S, Welte S, et al. A quantum-logic gate between distant quantum-network modules. Science 2021;371:614.
[33] Wang X-L, Cai X-D, Su Z-E, et al. Quantum teleportation of multiple degrees of freedom of a single photon. Nature 2015;518:516.
[34] Zhang Y, Agnew M, Roger T, et al. Simultaneous entanglement swapping of multiple orbital angular momentum states of light. Nat Commun 2017;8:632.
[35] Hu X-M, Zhang C, Liu B-H, et al. Experimental high-dimensional quantum teleportation. Phys Rev Lett 2020;125:230501.
[36] Luo Y-H, Zhong H-S, Erhard M, et al. Quantum teleportation in high dimensions. Phys Rev Lett 2019;123:070505.
[37] Wu Y, Wang Q, Tian L, et al. Multi-channel multiplexing quantum teleportation based on the entangled sideband modes. Photon Res 2022;10:1909.
[38] Liu S, Lou Y, Jing J, et al. Orbital angular momentum multiplexed deterministic all-optical quantum teleportation. Nat Commun 2020;11:3875.
[39] Liu S, Lou Y, Chen Y, et al. All-optical entanglement swapping. Phys Rev Lett 2022;128:060503.
[40] Liu S, Lv Y, Wang X, et al. Deterministic all-optical quantum teleportation of four degrees of freedom. Phys Rev Lett 2024;132:100801.
[41] Zhang TC, Goh KW, Chou CW, et al. Quantum teleportation of light beams. Phys Rev A 2003;67:033802.
[42] Yonezawa H, Furusawa A, Van Loock P, et al. Sequential quantum teleportation of optical coherent states. Phys Rev A 2007;76:032305.
[43] Takei N, Aoki T, Koike S, et al. Experimental demonstration of quantum teleportation of a squeezed state. Phys Rev A 2005;72:042304.
[44] Yonezawa H, Braunstein SL, Furusawa A, et al. Experimental demonstration of quantum teleportation of broadband squeezing. Phys Rev Lett 2007;99:110503.
[45] Lee N, Benichi H, Takeno Y, et al. Teleportation of nonclassical wave packets of light. Science 2011;332:330.
[46] Fuwa M, Toba S, Takeda S, et al. Noiseless conditional teleportation of a single photon. Phys Rev Lett 2014;113:223602.
[47] Weedbrook C, Pirandola S, García-Patrón R, et al. Gaussian quantum information. Rev Mod Phys 2012;84:621.
[48] Liu S, Han D, Wang N, et al. Experimental demonstration of remotely creating Wigner negativity via quantum steering. Phys Rev Lett 2022;128:200401.
[49] Han D, Sun F, Wang N, et al. Remote preparation of optical cat states based on Gaussian entanglement. Laser Photon Rev 2023;17:2300103.
[50] Wang M, Xiang Y, Kang H, et al. Deterministic distribution of multipartite entanglement and steering in a quantum network by separable states. Phys Rev Lett 2020;125:260506.
[51] Deng X, Xiang Y, Tian C, et al. Demonstration of monogamy relations for Einstein-Podolsky-Rosen steering in Gaussian cluster states. Phys Rev Lett 2017;118:230501.
[52] Braunstein SL, Fuchs CA, Kimble HJ, et al. Quantum versus classical domains for teleportation with continuous variables. Phys Rev A 2001;64:022321.
[53] Grosshans F, Grangier P. Quantum cloning and teleportation criteria for continuous quantum variables. Phys Rev A 2001;64:010301.